

W. MOĆKO\*,\*\*

## COMPARISON OF ENERGY ABSORPTION PROPERTIES OF HIGH NITROGEN AUSTENITIC STEEL AND CAST ALLOY DETERMINED USING LOW VELOCITY PERFORATION TEST

### PORÓWNANIE WYZNACZONYCH W TRAKCIE PRÓBY PRZEBIJANIA ENERGOCŁONNYCH WŁAŚCIWOŚCI STALI AUSTENITYCZNEJ ORAZ STALIWA O WYSOKIEJ ZAWARTOŚCI AZOTU

The results of energy absorbing analysis of VP159 austenitic steel and LH556 cast alloy were presented in this article. The assessment was carried out on the basis of drop-weight tower perforation test at impact energy equal to 500J and striker velocity equal to 12,5 m/s. Moreover, the basic mechanical properties of both tested materials were estimated in order to calibrate coefficients of the Johnson-Cook visco-plasticity model and Johnson-Cook damage initialization criterion as well. Subsequently, both models were applied for the finite element method simulation of perforation process. The reasonable agreement between measured and calculated shape of energy absorption curves were obtained for steel and cast alloy as well.

*Keywords:* Energy absorption, austenitic steel, cast alloy, constitutive modeling, damage initiation criterion

W pracy przedstawiono wyniki analizy zdolności do pochłaniania energii blach wykonanych ze stali austenitycznej typu VP159 oraz staliwa LH556. Ocenę przeprowadzono wykorzystując test przebijania wykonany z użyciem młota opadowego przy energii uderzenia 500J i prędkości iglicy równej 12,5 m/s. Dodatkowo wyznaczono także charakterystyki mechaniczne obu materiałów. Na tej podstawie dokonano kalibracji modelu lepko-plastyczności Johnsona-Cooka oraz oszacowano kryterium inicjalizacji uszkodzenia Johnsona-Cooka. Następnie modele zostały wykorzystane do symulacji procesu przebijania z użyciem MES. Zarówno dla stali jak i staliwa uzyskano dobrą zgodność pomiędzy zmierzonymi i obliczonymi krzywymi pochłaniania energii.

## 1. Introduction

Austenitic steels due to excellent mechanical properties such as high work hardening exponent and high, positive value of strain rate sensitivity are often used in many kinds of energy absorbing structures [1, 2] including ballistic shields. Therefore, many papers concerning analysis of steel sheet perforation may be found [3-7]. During those researches various experimental conditions were applied i.e. projectiles were ended with blunt, conical and spheroidal shape; different impact velocity was used ranging from 2,5 m/s to 600 m/s as well as various sheet thicknesses was applied.

This article presents assessment of the energy absorbing capabilities of austenitic steel determined using low velocity perforation test. Obtained results were compared with values estimated for cast alloy, which also may be applied as a component of armor [3]. The analysis were carried out on the example of VP159 austenitic steel and LH556 cast alloy with high content of nitrogen. The chemical composition of both materials was presented in Table 1. The steel was delivered in a form of 3 mm thickness sheet, whereas cast alloy in a form of cast.

TABLE 1  
The chemical composition of the tested material

	C [%]	Si [%]	Cr [%]	Mn [%]	N <sub>2</sub> [%]
VP159	0.04	0.30	16.50	12.00	0.61
LH556	0.16	0.44	21.40	15.21	1.13

## 2. Estimation of energy absorbing properties using perforation tests

The analysis of energy absorbing capabilities of tested materials was carried out using drop weight impact test system fabricated by Instron company. The specimens of 35 mm square shape were cut of 3 mm sheets. Subsequently, the specimens were placed on the anvil with circular aperture of 20 mm diameter and clamped by the holdfast. During the test, the axially symmetric striker, loaded with additional mass in order to reach the impact energy equal to 500J, was accelerated to 12,5 m/s and hit the tested specimen, and as a consequence caused material perforation. The striker of 10 mm in diameter was

\* INSTITUTE OF FUNDAMENTAL TECHNOLOGICAL RESEARCH, POLISH ACADEMY OF SCIENCE, STR. PAWIŃSKIEGO 5B, 02-106 WARSAW, POLAND  
 \*\* MOTOR TRANSPORT INSTITUTE, 80 JAGIELLOŃSKA STR., 03-301 WARSZAWA, POLAND

made of maraging steel rod. Shape of the striker was conical with rounded tip of 2 mm radius. The drop-weight tower was equipped with measurement system in order to acquire force and absorbed energy curves during impact. View of the striker and anvil was presented in Fig. 1.



Fig. 1. View of striker and anvil

The impact energy equal to 500 J was high enough to cause perforation of the specimen in the case of VP159 steel and LH556 cast alloy as well. View of the specimen after completion of the test carried out using drop-weight tower was presented in Fig. 2. In the case of VP159 steel (Fig.2a) strong plastic deformation near impact zone may be observed as well as formation of characteristic flakes due to tensile and shear loadings [5]. In the case of LH556 cast alloy (Fig.2b) the perforation mechanism was different. Due to low ductility of cast alloy many cracks were formed in material. As a consequence the reason of occurrence and enlargement of aperture in this material was spalling of subsequent material pieces.

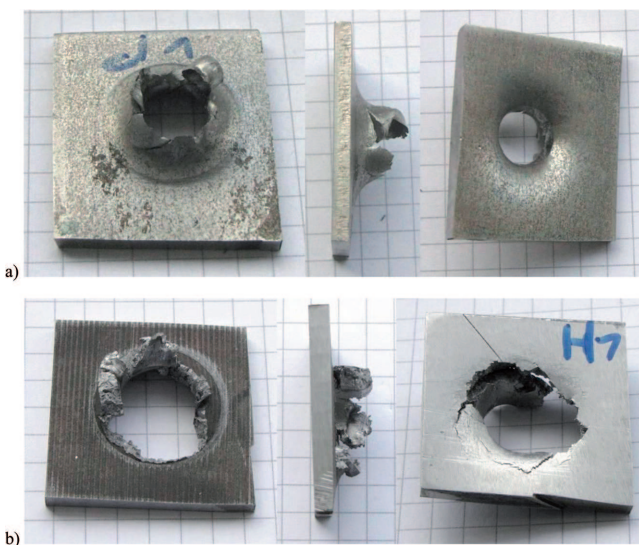


Fig. 2. View of the specimen after the perforation test: a) VP159 steel VP159; b) LH556 cast alloy

Optical micrographs of the specimen cross-sections made of VP159 steel after impact for was presented in Fig. 3. The photos show the area of crack initiation near the specimen axis. It may be observed that near the crack zone, strongly deformed grains contain clearly visible slip band and twins.

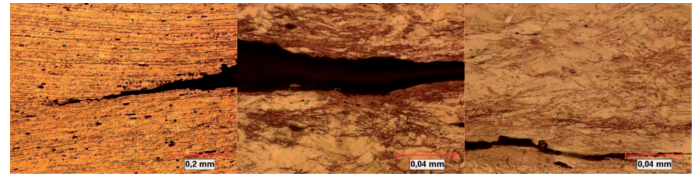


Fig. 3. Microstructure of specimen made of VP 159 steel after the perforation test

The view of the specimen cross-section made of LH556 cast alloy was shown in Fig. 4. It may be observed that material microstructure consists of two phases. During plastic deformation of material the phase of dendritic shape is damaged, and as a consequence macroscopic damage of material is observed. It may be the possible reason of cast alloy spalling during perforation process.

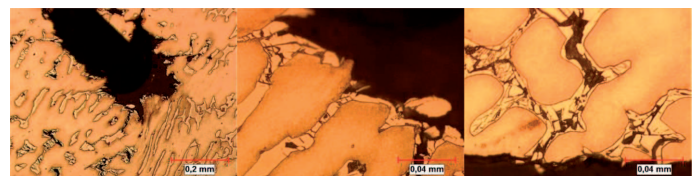


Fig. 4. Microstructure of specimen made of LH556 cast alloy after the perforation test

### 3. Constitutive modeling and FEM simulation of perforation test

An analysis of basic mechanical properties of tested materials was carried out in order to simulate process of perforation. The analysis involved the determination of stress-strain curves under quasi-static tensile and compressive loading conditions. Then, the experiment using split Hopkinson pressure bar (SHPB) [8] was carried out to estimate the strain rate sensitivity of both materials. After that, the steel and cast alloy in “as-received” state and after compression applied during SHPB test were analyzed using optical microscope. Then, the results of mechanical properties analysis were applied to calibrate Johnson-Cook’s constitutive equation and to determine Johnson-Cook’s damage initiation criterion. Finally the material models were used in FEM simulation of perforation test.

#### 3.1. Analysis of mechanical properties of tested materials

In the first stage of mechanical behavior analysis the quasi-static tensile test was carried out. Obtained stress-strain curves were presented in Fig. 5a) for VP159 steel and Fig. 5b) for LH556 cast alloy. VP159 steel shows good ductility, which results in elongation at break equal to 0.45 and high work hardening exponent as well. In the case of LH556 cast alloy, specimen failure was obtained at very low strain value,

thus it was hard to determine work hardening exponent under tensile loadings for strain higher than 0.015.

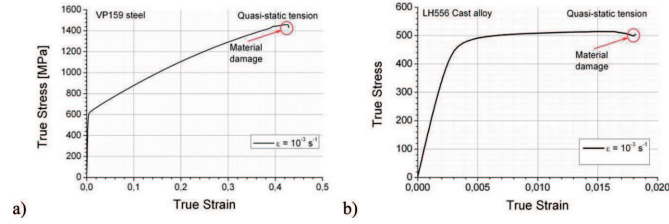


Fig. 5. Stress-strain curves at quasi-static tensile loading conditions: a) VP159 steel; b) LH556 cast alloy

The results of compression tests carried out at wide range of strain rates within the range from  $3,2 \times 10^{-3} \text{ s}^{-1}$  to  $5,0 \times 10^3 \text{ s}^{-1}$  were presented in Fig. 6a) for VP159 steel and 6b) for LH556 cast alloy. The experiments at quasi-static deformation regime were done by servo-hydraulic testing machine, whereas tests at dynamic loading conditions were carried out using Hopkinson bar [9]. Next, methodology described in details in previous works [10–12] was applied in order to correct effects of friction, inertia and adiabatic heating on the results acquired at high strain rate compressive loadings. Clearly visible work hardening effect may be found in both tested materials. It is worth to emphasize that no macroscopic damages were noticed in compressive tests at strains up to 0.4, despite very low ductility of this material in tensile test.

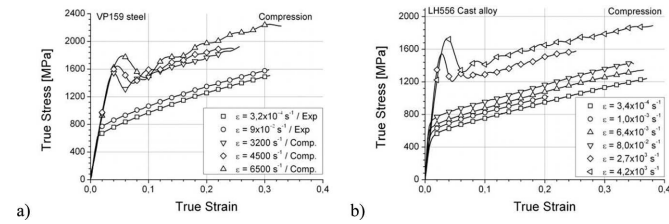


Fig. 6. Stress-strain curves at compressive loading conditions at wide range of strain rates: a) VP159 steel; b) LH556 cast alloy

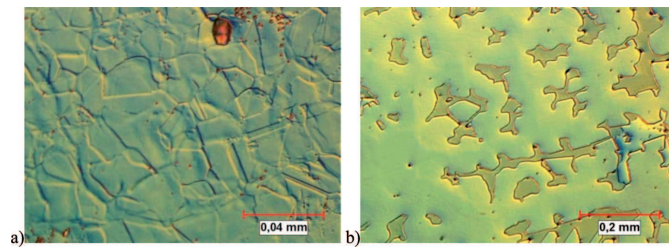


Fig. 7. Microstructure of tested materials in as-received state: a) VP159 steel; b) LH556 cast alloy

The view of microstructure of examined materials obtained using optical microscope was presented in Fig. 7 for “as-received” materials and in Fig. 8 for materials after dynamic compression test. In the case of VP159 steel (Fig. 7a) the structure containing grains and twins introduced during steel fabrication process may be observed. In this same material after Hopkinson bar test (Fig. 8a) the clearly visible slip bands may be noticed as a result of plastic deformation. Microstructure of LH556 cast alloy in “as-received” state consists of two phases (Fig. 7b). As a consequence of plastic deformation

the phase of dendritic shape is crushed, whereas in the second phase you may observe slip bands (Fig. 8b).

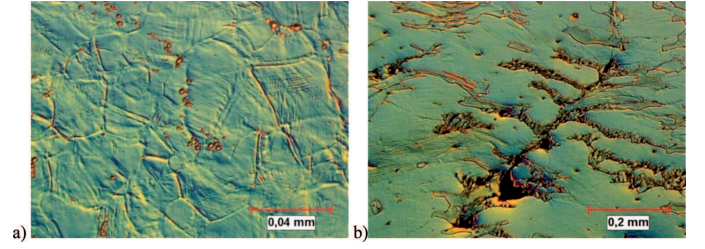


Fig. 8. Microstructure of tested materials after SHPB compression test: a) VP159 steel; b) LH556 cast alloy

### 3.2. Calibration of Johnson-Cook’s constitutive model

In order to describe visco-plastic properties of tested materials the Johnson-Cook’s (JC) constitutive model [13] was applied. The plastic flow stress in this equation may be presented as a function of the strain, the strain rate and the temperature in the multiplicative form as follows:

$$\sigma(\epsilon, \dot{\epsilon}, T) = (A + B\epsilon^n) \left( 1 + C \ln \left( \frac{\dot{\epsilon}}{\dot{\epsilon}_0} \right) \right) \left( 1 - \left( \frac{T - T_R}{T_m - T_R} \right)^m \right), \quad (1)$$

where

A – yield point in the reference conditions: temperature  $T_R$  and strain rate; B, n – strain-hardening exponents; C – dynamic hardening exponent; m – thermal softening coefficient;  $T_m$  – melting point.

The results of constitutive model coefficient calibration carried out using Origin 8. 1 software on the basis of experimental characterization were presented in Table 2.

TABLE 2  
Coefficients of the JC constitutive model

	A [MPa]	B [MPa]	n	C	m	$\epsilon_0$ [s <sup>-1</sup> ]	$T_R$ [K]	$T_m$ [K]
VP159	525	2230	0.7	0.037	0.6	$3 \times 10^{-4}$	296	1,800
LH556	500	1650	0,8	0,05	0.6	$3 \times 10^{-4}$	296	1,800

### 3.3. Johnson-Cook’s damage initiation criteria

To model the material damage initiation, the Johnson-Cook criterion was used [14], which can be expressed in the form of the following equation:

$$\bar{\epsilon}_D^{pl} = [d_1 + d_2 \exp(-d_3 \eta)] \left[ 1 + d_4 \ln \left( \frac{\dot{\epsilon}}{\dot{\epsilon}_0} \right) \right] (1 + d_5 \hat{\theta}) \quad (2)$$

where:

$$\hat{\theta} \equiv \begin{cases} 0 & \text{for } \theta < \theta_{TRANS} \\ (\theta - \theta_{TRANS}) / (\theta_{MELT} - \theta_{TRANS}) & \text{for } \theta_{TRANS} \leq \theta \leq \theta_{MELT} \\ 1 & \text{for } \theta > \theta_{MELT} \end{cases}$$

– value of the plastic strain at which the damage occurs;  $d_1$ – $d_5$  – coefficients of damage;  $\eta$  – stress triaxiality;  $\theta_{MELT}$  – melting point;  $\theta_{TRANS}$  – transition temperature;  $\theta$  – current temperature; and – reference strain rate.



Coefficients of eqn. (2) were determined on the basis of quasi-static tensile tests and data taken from previous works concerning influence of stress triaxiality on the damage initiation in steels [15]. The results of calibration were presented in Table 3.

TABLE 3  
Coefficients of JC damage initiation criteria

	$d_1$	$d_2$	$d_3$	$d_4$	$d_5$	$\theta_{\text{TRANS}}$	$\theta_{\text{MELT}}$	$^{-1}_{[s]}$
VP159	0,35	0,7	3	-0.0123	0	300	1,600	0.0005
LH556	0,015	0,3	4	-0.0123	0	300	1,600	0.0005

### 3.4. FEM simulation of perforation test

A computer simulation of the perforation test was performed in the ABAQUS/Explicit environment [16]. To model the plastic behaviour of the material, the constitutive equations discussed in the previous section of this paper were used. The following material constant were assumed for steel: density of  $7,800 \text{ kg/m}^3$ ; Young's modulus of  $205 \text{ GPa}$ ; Poisson's coefficient of  $0.3$ ; inelastic heat fraction of  $0.9$ ; specific heat of  $475 \text{ J/(kgK)}$ . For the purpose of simulation, it was assumed that the striker and the anvil are perfectly rigid bodies. The view of testing stand was presented in Fig. 9.

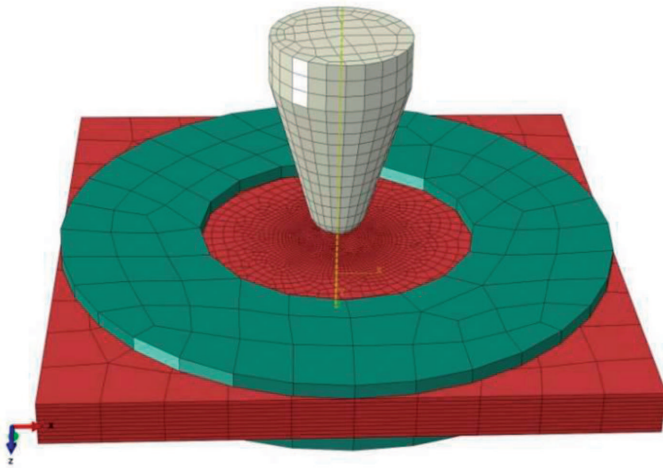


Fig. 9. FEM model of the specimen and testing stand

The distribution of Huber-Mises stress in specimens after the perforation process, determined using FEM was presented in Fig. 10 for VP159 steel and Fig. 11 for LH556 cast alloy. In both cases the numerically determined view of specimens were in good agreement with those of experiments shown in Fig. 2a and Fig. 2b. For VP159 steel strong plastic deformation near area of striker impact and flakes formation may be found, as well. Whereas for LH556 cast alloy a number of cracks in the material and its spalling was noticed.

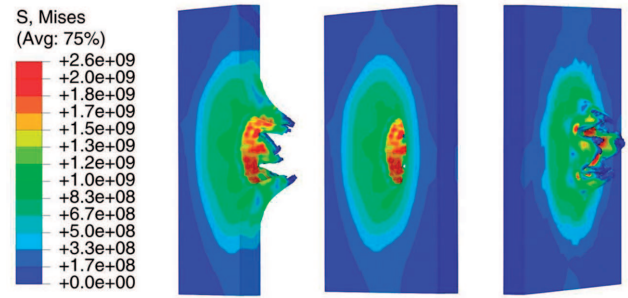


Fig. 10. Results of FEM simulation of VP159 steel perforation tests

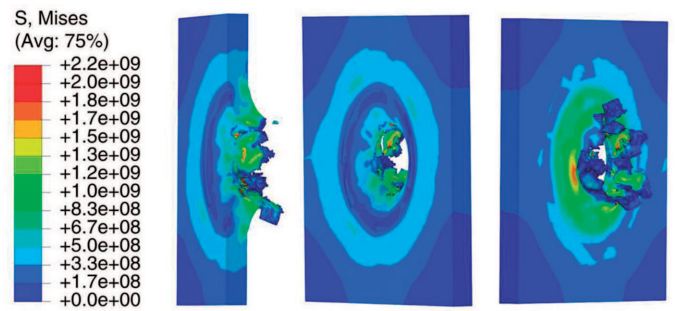


Fig. 11. Results of FEM simulation of LH556 cast alloy perforation tests

The chart containing absorbed energy during the perforation test is presented in Fig. 12 a) for VP159 steel and 12b) for LH556 cast alloy, respectively. The experimentally obtained curves shows reasonable agreement with computer simulation results, thus constitutive model and damage initiation criterion were properly chosen and calibrated. The value of energy absorbed by specimen made of steel is higher ( $480 \text{ J}$ ) in comparison to energy absorbed by cast alloy ( $350 \text{ J}$ )

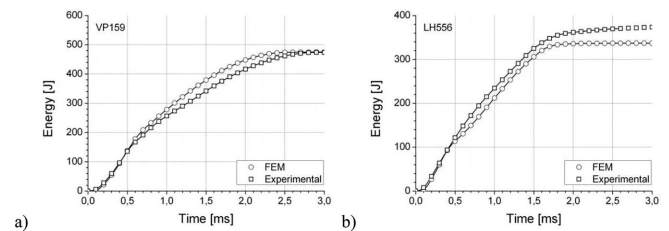


Fig. 12. Measured and calculated using FEM energy absorbed during perforation test: a) VP159 steel; b) LH556 cast alloy

## 4. Conclusions

The following conclusions may be drawn on the basis of microstructural and mechanical properties analysis and FEM simulations:

- Mechanical properties of both materials such as: work hardening exponent and strain rate sensitivity are comparable. The only significant difference was found in the value of elongation. Very low elongation for cast alloy is caused by presence of hard and brittle phase in material microstructure. It results in fast damage initiation and rupture of a specimen.

- VP159 steel shows better energy absorbing properties in comparison with LH556 cast alloy. However this difference is not so significant, taking into account strong discrepancy in elongation value during tensile test for both materials.
- In case of steel, the enlargement of aperture during striker impact takes place by plastic deformation and flakes formation, whereas in the case of cast alloy, the aperture enlargement is the result of spalling of subsequent specimen fragments.

#### REFERENCES

- [1] W. Moćko, *Journal of KONES* **19**, 305-310 (2012).
- [2] W. Moćko, Z.L. Kowalewski, *Proceedings of the 15th International Conference on Experimental Mechanics*, Porto, Portugal, Edicoes INEGI, 1145-46 (2012).
- [3] J. Dean, C.S. Dunleavy, P.M. Brown, T.W. Clyne, *Int. J. Impact Eng.* **36**, 1250-1258 (2009).
- [4] T. Borvik, M. Langseth, O.S. Hopperstad, K.A. Malo, *Int. J. Impact Eng.* **27**, 37-64 (2002).
- [5] J.A. Rodriguez-Martinez, A. Rusinek, R. Pesci, *Thin Wall. Struct.* **48**, 966-978 (2010).
- [6] A. Rusinek, J.A. Rodriguez-Martinez, P.R. Zazera, J.R. Klepaczko, A. Arias, C. Asuvelet, *Int. J. Impact Eng.* **36**, 565-587 (2009).
- [7] T. Kursun, *Arch. Metall. Mater.* **56**, 955-963 (2011).
- [8] W. Moćko, Z.L. Kowalewski, A. Wojciechowski, D. Rudnik, *Biuletyn WAT* **61**, 449-462 (2012).
- [9] H. Kolsky, *Proc. Phys. Soc.* **62B**, 676 (1949).
- [10] W. Moćko, Z.L. Kowalewski, *Engineering Transactions* **59**, 1-14 (2011).
- [11] W. Moćko, J.A. Rodriguez-Martinez, Z.L. Kowalewski, A. Rusinek, *Strain* **48**, 498, doi:10.1111/j.1475-1305.2012.00847.x (2012).
- [12] W. Moćko, Z.L. Kowalewski, *Transport Samochodowy* **32**, 97-105 (2011).
- [13] G.R. Johnson, W.H. Cook, *Proceedings of Seventh International Symposium on Ballistics*, The Hague, The Netherlands, 1983.
- [14] G.R. Johnson, W.H. Cook, *Eng. Fract. Mech.* **21**, 31-48 (1985).
- [15] G. Trattnig, T. Antretter, R. Pippa, *Eng. Fract. Mech.* **75**, 223-235 (2008).
- [16] M. Wojtaszek, P. Chyła, T. Śleboda, A. Łukaszek-Sołek, S. Bednarek, *Arch. Metall. Mater.* **56**, 627-635 (2012).

*Received: 20 September 2013.*